Calcium/calmodulin-dependent kinase II and nitric oxide synthase 1 dependent modulation of ryanodine receptors during β-adrenergic stimulation is restricted to the dyadic cleft.

Dries, Eef; Santiago, Demetrio J.; Johnson, Daniel M.; Gilbert, Guillaume; Holemans, Patricia; Korte, Sanne M.; Roderick, H. Llewelyn; Sipido, Karin R.

DOI:
10.1113/JP271965

Document Version
Publisher's PDF, also known as Version of record

Citation for published version (Harvard):
Dries, E, Santiago, DJ, Johnson, DM, Gilbert, G, Holemans, P, Korte, SM, Roderick, HL & Sipido, KR 2016, 'Calcium/calmodulin-dependent kinase II and nitric oxide synthase 1 dependent modulation of ryanodine receptors during β-adrenergic stimulation is restricted to the dyadic cleft.', *The Journal of Physiology*, vol. 594, no. 20, pp. 5923-5939. https://doi.org/10.1113/JP271965

J Physiol 594.20 (2016) pp 5923–5939

The Journal of Physiology

Calcium/calmodulin-dependent kinase II and nitric oxide synthase 1-dependent modulation of ryanodine receptors during β-adrenergic stimulation is restricted to the dyadic cleft

Eef Dries, Demetrio J. Santiago, Daniel M. Johnson, Guillaume Gilbert, Patricia Holemans, Sanne M. Korte, H. Llewelyn Roderick and Karin R. Sipido

Experimental Cardiology, Department of Cardiovascular Sciences, KU Leuven, Belgium

Key points

- The dyadic cleft, where coupled ryanodine receptors (RyRs) reside, is thought to serve as a microdomain for local signalling, as supported by distinct modulation of coupled RyRs dependent on Ca^{2+}/calmodulin-dependent kinase II (CaMKII) activation during high-frequency stimulation.
- Sympathetic stimulation through β-adrenergic receptors activates an integrated signalling cascade, enhancing Ca^{2+} cycling and is at least partially mediated through CaMKII.
- Here we report that CaMKII activation during β-adrenergic signalling is restricted to the dyadic cleft, where it enhances activity of coupled RyRs thereby contributing to the increase in diastolic events. Nitric oxide synthase 1 equally participates in the local modulation of coupled RyRs.
- In contrast, the increase in the Ca^{2+} content of the sarcoplasmic reticulum and related increase in the amplitude of the Ca^{2+} transient are primarily protein kinase A-dependent.
- The present data extend the concept of microdomain signalling in the dyadic cleft and give perspectives for selective modulation of RyR subpopulations and diastolic events.

Abstract In cardiac myocytes, β-adrenergic stimulation enhances Ca^{2+} cycling through an integrated signalling cascade modulating L-type Ca^{2+} channels (LTCCs), phospholamban and ryanodine receptors (RyRs). Ca^{2+}/calmodulin-dependent kinase II (CaMKII) and nitric oxide synthase 1 (NOS1) are proposed as prime mediators for increasing RyR open probability. We investigate whether this pathway is confined to the high Ca^{2+} microdomain of the dyadic cleft and thus to coupled RyRs. Pig ventricular myocytes are studied under whole-cell voltage-clamp and confocal line-scan imaging with Fluo-4 as a $[Ca^{2+}]_i$ indicator. Following conditioning depolarizing pulses, spontaneous RyR activity is recorded as Ca^{2+} sparks, which are assigned to coupled and non-coupled RyR clusters. Isoproterenol (ISO) (10 nM) increases Ca^{2+} spark frequency in both populations of RyRs. However, CaMKII inhibition reduces spark frequency in coupled RyRs only; NOS1 inhibition mimics the effect of CaMKII inhibition. Moreover, ISO induces the repetitive activation of coupled RyR clusters through CaMKII activation. Immunostaining shows high levels of CaMKII phosphorylation at the dyadic cleft. CaMKII inhibition reduces I_{CaL} and local Ca^{2+} transients during depolarizing steps but has only modest effects on amplitude or relaxation of the global Ca^{2+} transient. In contrast, protein kinase A (PKA) inhibition reduces spark frequency in all RyRs concurrently with a reduction of sarcoplasmic reticulum Ca^{2+} content, Ca^{2+} transient amplitude and relaxation. In conclusion, CaMKII activation during β-adrenergic stimulation is restricted to the dyadic cleft microdomain, enhancing LTCC-triggered local Ca^{2+} release as well as spontaneous diastolic Ca^{2+} release whilst PKA is the major pathway increasing global Ca^{2+} cycling. Selective CaMKII inhibition may reduce potentially arrhythmogenic release without negative inotropy.

DOI: 10.1113/JP271965

(Received 30 November 2015; accepted after revision 17 April 2016; first published online 28 April 2016)
Corresponding author K. R. Sipido: Experimental Cardiology, KU Leuven, Campus Gasthuisberg, Herestraat 49, B-3000 Leuven, Belgium. Email: Karin.Sipido@kuleuven.be

Abbreviations AC, adenylate cyclase; AIP, autocamtide-2-related-inhibitory-peptide; β-AR, β-adrenergic receptor; CaMKII, Ca^{2+}/calmodulin-dependent kinase II; CPVT, catecholaminergic polymorphic ventricular tachycardia; Epac, exchange protein activated by cAMP; I_{CaL}, L-Type Ca^{2+} current; ISO, isoproterenol; LTCC, L-type Ca^{2+} channel; L-VNIO, vinyl-L-NIO hydrochloride; LV, left ventricle; NAC, *N*-acetylcysteine; NCX, Na^+/Ca^{2+} exchanger; NO, nitric oxide; NOS1, nitric oxide synthase1; P_o, open probability; PDE, phosphodiesterase; PKA, protein kinase A; PKI, protein-kinase inhibitor; PLN, phospholamban; ROS, reactive oxygen species; RyR, ryanodine receptor; SERCA, SR Ca^{2+}-ATPase; SR, sarcoplasmic reticulum; T_{F50}, time to reach half-maximal $[Ca^{2+}]_i$; TT, T-tubule.

Introduction

In the heart, inotropy, lusitropy and chronotropy are increased by catecholamine-mediated activation of β-adrenergic receptors (β-ARs), for example during emotional stress or physical exercise. This results in increased cardiac output to meet the metabolic demand, and this adaptation is largely due to modulation of myocyte Ca^{2+} handling. Upon activation, β-ARs stimulate adenylate cyclase (AC) via G proteins to produce cAMP. Activation of the cAMP-dependent kinase protein kinase A (PKA) leads to the phosphorylation of several Ca^{2+} handling proteins: L-type Ca^{2+} channels (LTCCs), resulting in enhanced L-type Ca^{2+} current (I_{CaL}); ryanodine receptors (RyRs), facilitating Ca^{2+} release from the sarcoplasmic reticulum (SR); and phospholamban (PLN), reducing inhibition of the SR Ca^{2+}-ATPase (SERCA) leading to an enhancement of Ca^{2+} uptake into the SR. The integrated response, larger and faster contraction and relaxation at higher heart rates, is the result of both frequency-dependent modulation of Ca^{2+} handling and direct β-receptor-mediated signalling.

β-AR-dependent RyR phosphorylation has recently received particular attention because of the association of RyR mutations with catecholaminergic polymorphic ventricular tachycardia (CPVT) and sudden death (Venetucci *et al.* 2012). *In vitro*, PKA-mediated phosphorylation at serine 2809 in RyR2 enhances RyR open probability (P_o), with one possible mechanism being the dissociation of the immunophilin FKBP12.6 from the RyR (Marx *et al.* 2000). However, this mechanism has been questioned and the exact mechanisms behind PKA regulation of RyRs in the intact cell, as well as its role in the β-AR response, remain controversial (Xiao *et al.*, 2004, 2006; Morimoto *et al.* 2009; Shan *et al.* 2010).

In addition to PKA, Ca^{2+}/calmodulin-dependent kinase II (CaMKII) is activated downstream of β-AR and also increases RyR P_o when measured as SR Ca^{2+} leak. This was shown in small rodents, guinea pigs and rabbits (Curran *et al.* 2007; Ferrero *et al.* 2007; Ogrodnik & Niggli, 2010). CaMKII activation was at first ascribed to PKA-dependent increases in $[Ca^{2+}]_i$. However, CaMKII activity can also be increased via mechanisms distinct from PKA during β-adrenergic stimulation (Pereira *et al.* 2007; Gutierrez *et al.* 2013; Curran *et al.* 2014). These findings have shifted the paradigm and CaMKII is viewed as a primary integrator of both frequency-dependent signalling and β-adrenergic signalling (rather than a secondary player, dependent on PKA).

At the molecular level, the exchange protein activated by cAMP (Epac) is a pathway for cAMP signalling that is independent of PKA (Ruiz-Hurtado *et al.* 2013). Stimulation of Epac, using the specific activator 8-CPT, led to an increased diastolic SR Ca^{2+} leak via CaMKII-dependent phosphorylation of serine 2814 in RyR2 (RyR-S2814) in myocytes from rat and mice hearts (Pereira *et al.*, 2007, 2013). Additionally, direct activation of CaMKII by nitric oxide (NO) during β-adrenergic stimulation has been reported to occur in non-paced cells, i.e. in the absence of increased Ca^{2+} transients (Gutierrez *et al.* 2013; Curran *et al.* 2014).

Other proteins that contribute to the overall β-adrenergic-mediated increase in Ca^{2+} cycling are PLN and sarcolemmal LTCCs. These proteins are phosphorylated in a PKA-dependent manner, which can be mimicked by forskolin, a direct activator of AC (Curran *et al.* 2007). Nevertheless, these proteins can also be modulated by CaMKII as part of the frequency-dependent modulation (Wu *et al.* 2012).

Recent studies have emphasized that β-adrenergic signalling is not necessarily homogeneous through the cardiac myocyte. Using fluorescence resonance energy transfer-based sensors, localized cAMP signalling in sub-cellular compartments was demonstrated (Zaccolo & Pozzan, 2002; Nikolaev *et al.* 2006; Agarwal *et al.* 2014). Such compartmentalized cAMP (and cGMP) signalling is associated with subcellular localization of different phosphodiesterases (PDEs) that restrict cAMP diffusion and the dimension of the cAMP microdomain (Leroy *et al.* 2008; Mika *et al.* 2014). In addition, different β-AR isoforms have specific subcellular locations and downstream targets (Gorelik *et al.* 2013). Local β-adrenergic signalling compartments are reported to be localized to T-tubules (TTs) and caveolae, where key components of the β-AR cascade are also found (e.g. G_s proteins, AC, PDE3/4 and AKAPs).

We recently reported on the role of CaMKII microdomains around RyRs in the response to increased stimulation frequency in the absence of β-AR stimulation (Dries *et al.* 2013). CaMKII-dependent potentiation of RyR activity was restricted to RyRs in the dyadic cleft (coupled RyRs), where there is a distinct Ca^{2+} microdomain, and absent in the RyRs not coupled to the sarcolemmal membrane (non-coupled RyRs) despite the fact that CaMKII was present in both locations.

The primary aim of the present study is to investigate whether modulation of RyRs through activation of the β-adrenergic receptor is restricted to the coupled RyRs in the microdomain of the dyadic cleft. Second, we examine the mechanisms underlying the regulation of RyRs during β-adrenergic stimulation. Finally, we investigate how microdomain CaMKII activation integrates with PKA signalling and global Ca^{2+} cycling. For our studies, we use pig ventricular myocytes that have a less dense TT network than rodents, more similar to that found in human ventricular myocytes (Heinzel *et al.* 2002; Louch *et al.* 2004; Jayasinghe *et al.* 2012).

Methods

Animal care

Healthy pigs (40-45 kg) were housed and treated according to the European Directive 2010/63/EU. Experimental protocols were approved by the in-house ethical committee (*Ethische Commissie Dierproeven*, KU Leuven), with permit numbers P10139 and P14176.

Cell isolation

Animals were killed via an overdose of pentobarbital (100 mg kg^{-1}) under full anaesthesia (absence of deep reflexes), after which the heart was quickly excised. Single cardiomyocytes were enzymatically isolated from the mid-myocardial layer of the left ventricle (LV) as described before (Heinzel *et al.* 2002). A large wedge with the perfusing artery was prepared and the coronary artery was cannulated and perfused with a constant flow (4 ml min^{-1}) at 37 °C. To washout the remaining blood, the tissue was initially perfused with normal Tyrode (in mmol l^{-1}: NaCl 137, KCl 5.4, $MgCl_2$ 0.5, $CaCl_2$ 1.8, Na-HEPES 11.8 and glucose 10; pH 7.4). Next, the tissue was perfused with a Ca^{2+}-free Tyrode (in mmol l^{-1}: NaCl 130, KCl 5.4, KH_2PO_4 1.2, $MgSO_4$ 1.2, Na-HEPES 6, glucose 20; pH 7.2) followed by the enzymatic solution [collagenase A (Roche, Basel, Switzerland) and protease XIV (Sigma-Aldrich, St Louis, MO, USA) added to Ca^{2+}-free Tyrode] and after digestion, perfused with low Ca^{2+} Tyrode (0.18 mM $CaCl_2$ added to Ca^{2+}-free Tyrode). The digested tissue was minced, after which the suspension was filtered and the isolated myocytes were resuspended in normal Tyrode. Cells were allowed to recover for 1 h after isolation before starting experiments.

Electrophysiological recordings

Cells were studied under whole-cell voltage-clamp to record membrane currents (Axon 200B amplifier, Axon Instruments, Union City, CA, USA). Cells were constantly perfused with normal Tyrode at 37 °C and patch pipettes (2–3 MΩ) (GB 200-8P, Science Products, Hofheim, Germany) were filled with (in mmol l^{-1}): K^+-aspartate 120, NaCl 10, KCl 20, K-Hepes 10, MgATP 5, and K_5Fluo-4 0.05; pH 7.2. Ca^{2+} transients were elicited by depolarizing steps (200 ms) from –70 to + 10 mV at 0.5 Hz for 30 s. This low-frequency stimulation protocol was chosen to exclude frequency-dependent potentiation (Dries *et al.* 2013). Protocols were repeated in the absence and presence of isoproterenol (ISO; 10 nM). SR Ca^{2+} content was measured by integrating the inward Na^+/Ca^{2+} exchanger (NCX) current during fast caffeine application (10 mmol l^{-1} for 8 s) after a conditioning train at 0.5 Hz stimulation. I_{CaL} was measured during pulses from –70 to +10 mV while the fast Na^+ current was inhibited with 5 μM TTX and 200 μM lidocaine.

The PKA inhibitor PKI (PKI myristoylated-(14-22)-amide; Tocris Bioscience, Bristol, UK) was used at 20 μM with incubation for 30 min and included in the pipette solution. The PKA inhibitor H-89 (Sigma-Aldrich, St Louis, MO, USA) was used at 10 μM with pre-incubation for 15 min and then included in the pipette solution. AIP (CaMKII inhibitor; autocamtide-2-related-inhibitory-peptide; Tocris Bioscience) was used at 10 μM with pre-incubation for 1 h and included in the patch pipette. CE3F4 (kindly provided by Frank Lezoualc'h, INSERM, Toulouse, France) was used at 20 μM with pre-incubation for 30 min and included in the patch pipette. ESI-05 (4-methylphenyl-2, 4, 6- trimethylphenylsulfone, Biolog, Hayward, CA, USA) was used at 10 μM with pre-incubation for 15 min and included in the patch pipette and wash-on during the experiments. Vinyl-L-NIO hydrochloride (L-VNIO, Santa Cruz Biotechnology, Inc., Santa Cruz, CA, USA) was used at 100 μM with pre-incubation for 30 min and in the patch pipette. *N*-acetylcysteine (NAC, Sigma-Aldrich) was used at 10 mM with pre-incubation for 1 h and included in the patch pipette.

Ca^{2+} measurements, confocal microscopy and image analysis

$[Ca^{2+}]_i$ was reported by Fluo-4. Confocal line scan images were recorded using a Zeiss LSM 510 confocal system. Line scans were recorded at 650 Hz with a pixel size of

0.2–0.3 μm. Following the 30 s conditioning train with depolarizing steps at 0.5 Hz, spontaneous Ca^{2+} sparks were routinely observed (15 s recording at the holding potential of –70 mV). Sparks were detected using an automated spark analysis program based on the Cheng algorithm (Dries *et al.* 2013). Spark frequency was calculated and normalized to line length and time as number of sparks per 100 μm per second. When analysing spark frequency in coupled *vs.* non-coupled sites, the frequency was normalized to the line length of these sites. To define coupled (dyadic) and non-coupled (non-dyadic) release sites, an algorithm based on the time taken to reach 50% peak amplitude (T_{F50}) of the Ca^{2+} transient was used as described previously (Dries *et al.* 2013). Briefly, five consecutive Ca^{2+} transients on the line scan images were averaged and fluorescence was normalized to the diastolic $[Ca^{2+}]_i$ level (F/F_0). From the averaged transient, the T_{F50} was calculated for each pixel along the line to establish the spatial distribution of the timing of the Ca^{2+} release. T_{F50} values were used as markers for the distance to the membrane (Dries *et al.* 2013). In the averaged Ca^{2+} transient, pixels were categorized as a coupled release site (< 0.5 μm) when $T_{F50} < 18$ ms and a non-coupled release site (> 2 μm) when $T_{F50} > 27$ ms. Release sites with a T_{F50} between 18 and 27 ms were excluded so to have a clearly separated population of coupled and non-coupled RyRs. Ca^{2+} sparks were then assigned to coupled or non-coupled sites to define spark properties in each type of RyR site (Fig. 1*Aa*).

Phosphorylation assays

Freshly isolated myocytes were stimulated at 0.5 Hz for 15 min using a multichannel homebuilt stimulator controlled using Labview 6.0 (National Instruments, Austin, TX, USA) in the presence and absence of ISO (10 nM). After stimulation, cells were fixed with 2% paraformaldehyde and permeabilized with 0.4% Triton X-100 in PBS. Cells were washed three times and incubated with blocking buffer (BSA 4%, 0.1% Triton X-100 in PBS) for 1 h at room temperature. Primary antibodies were incubated overnight at 4°C (mouse IgG anti-RyR 1:200, MA3-925 from Thermo Scientific, Waltham, MA, USA; mouse IgM anti-NCX 1:200, MA3-926 from Thermo Scientific; rabbit IgG anti-phospho-CaMKII Th286 1:200, PA1-14076 from Thermo Scientific). Cells were washed three times in PBS and incubated with secondary antibodies (RyR: Alexa fluor 488 goat anti-mouse IgG; NCX: Alexa fluor 647 goat anti-mouse IgM; Phospho-CaMKII Th286: Alexa fluor 568 goat anti-rabbit IgG) diluted at 1:200 in blocking buffer for 2 h at room temperature. Cells were washed three times in PBS before imaging with a confocal microscope (Nikon A1R configured on an Eclipse Ti using a 60× 1.4 NA oil immersion objective). Fluorescence intensity was measured for phospho-CaMKII Th286 in the whole cell and local regions (coupled *vs.* non-coupled RyRs) using ImageJ. Whole-cell fluorescence was normalized to background; local regions are shown as ratio of fluorescence in coupled/non-coupled regions. Identification of coupled and non-coupled regions was performed by using a mask of the skeletonized NCX signals < 0.5 or > 2 μm away, respectively, as described previously (Dries *et al.* 2013).

Statistics

All data are presented as means ± SEM. Data have been compared using a paired Student's *t* test or a two-way ANOVA with Bonferroni *post hoc* testing when comparing a specific blocker in coupled *versus* non-coupled RyRs. Data were considered significantly different when $P < 0.05$ and is represented as $^{*}P < 0.05$, $^{**}P < 0.01$ and $^{***}P < 0.001$.

Results

During β-adrenergic stimulation sparks increase globally but only coupled RyRs are modulated by CaMKII

In the present study, spark frequency increased equivalently at both coupled and non-coupled RyRs after application of ISO (Fig. 1*Ab*). SR Ca^{2+} content was also increased following ISO stimulation (Fig. 1*Ac*). These data were somewhat unexpected as the literature suggests that CaMKII is the pathway for ISO-dependent modulation of RyR and we had hypothesized that CaMKII activation, and increase of sparks, would be restricted to the dyadic cleft and coupled RyRs. We therefore validated that the restricted modulation of coupled RyRs by CaMKII during high-frequency stimulation alone (cells conditioned at 2 Hz, no ISO; Dries *et al.* 2013) was intact (Fig. 2). Furthermore, global Ca^{2+} handling during β-adrenergic stimulation with ISO was also as previously described in many species, with increased amplitude of the Ca^{2+} transient and faster relaxation, larger ICaL and greater number of Ca^{2+} sparks (Fig. 3).

Having confirmed selective regulation of coupled RyRs by high-frequency stimulation, we next examined whether there was a specific CaMKII component to the global ISO response. Relative to ISO-treated cells, the specific CaMKII inhibitor AIP reduced the spark frequency in coupled RyRs by 50%, without affecting the frequency of sparks at the non-coupled RyRs (Fig. 1*Ba*) or the SR Ca^{2+} content (Fig. 1*Bb*). When the relationship between SR Ca^{2+} content and spark frequency was examined, the CaMKII-specific modulation of coupled RyRs occurred independently of changes in the SR Ca^{2+} content (Fig. 1*C*).

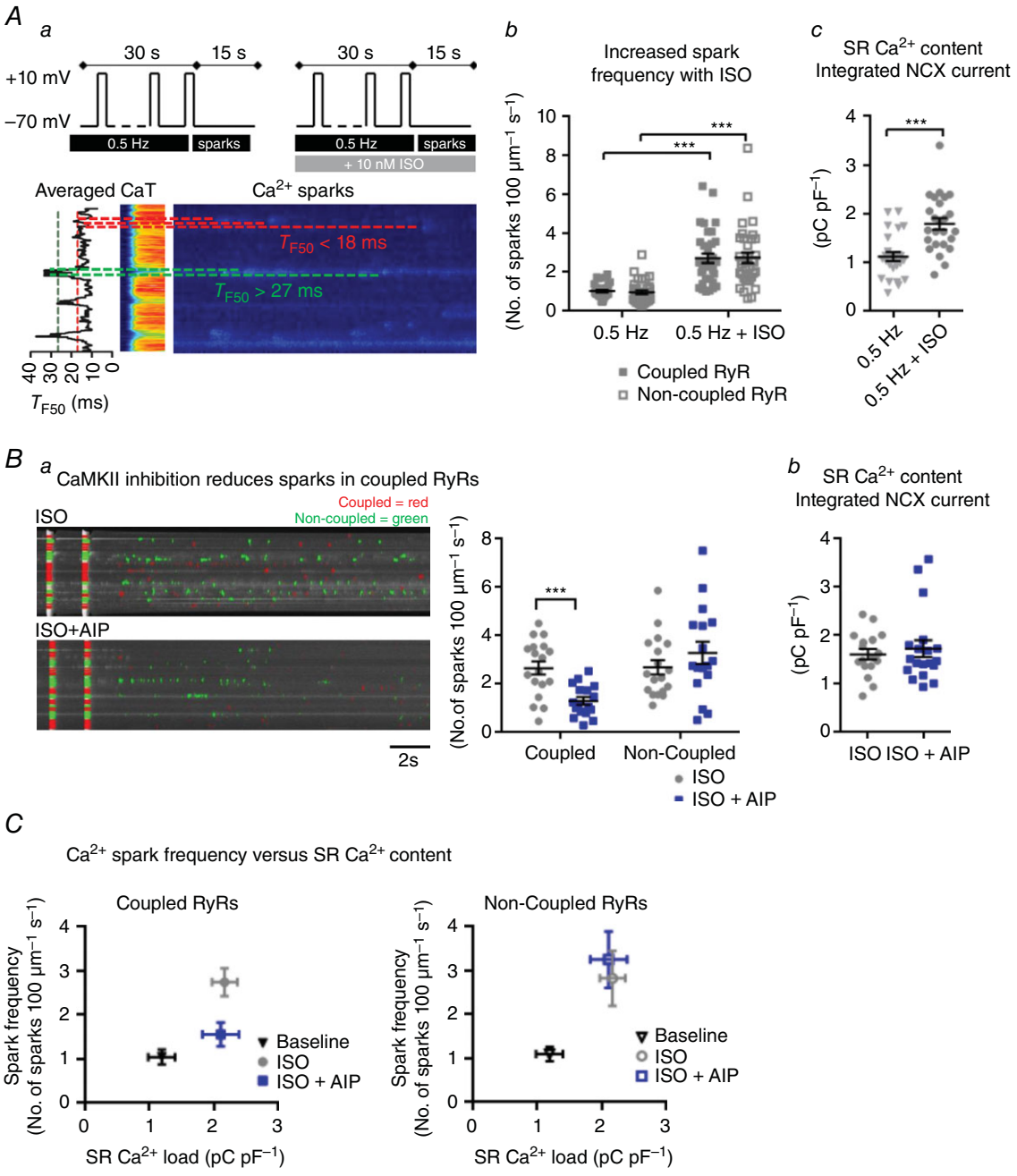

Figure 1. After ISO the spark frequency in both coupled and non-coupled RyRs is increased, but only coupled RyRs are modulated by CaMKII

Aa, myocytes are stimulated in the presence and absence of ISO using depolarizing steps (–70 to +10 mV; 200 ms) for 30 s at 0.5 Hz and Ca^{2+} sparks are recorded during a 15 s period after stimulation. Example of a confocal line scan image is shown. Ca^{2+} sparks are assigned to coupled and non-coupled using the temporal cut-off values of the averaged Ca^{2+} transients. Coupled sites ($< 0.5\ \mu$m) have a $T_{F50} < 18$ ms (shown in red) and non-coupled sites ($> 2\ \mu$m) have a $T_{F50} > 27$ ms (shown in green). *Ab*, spark frequency in coupled and non-coupled RyRs before and after ISO ($n_{cells} = 34$; $N_{pigs} = 11$); and *c*, SR Ca^{2+} content before and after ISO application ($n_{cells} = 25$; $N_{pigs} = 9$). *Ba*, example of a confocal line scan image showing Ca^{2+} transients and Ca^{2+} sparks in the presence of ISO and ISO with AIP. Ca^{2+} sparks originating from coupled regions are shown in red and from non-coupled regions in green. Ca^{2+} sparks from intermediate sites are not colour-coded. The effect of AIP on Ca^{2+} spark frequency in coupled and non-coupled RyRs after ISO ($n_{cells} = 17$; $N_{pigs} = 5$); *b*, effect of AIP on the SR Ca^{2+} content during ISO ($n_{cells} = 19$; $N_{pigs} = 5$). *C*, the relationship between SR Ca^{2+} load and Ca^{2+} sparks at baseline ($n_{cells} = 7$; $N_{pigs} = 6$), ISO ($n_{cells} = 10$; $N_{pigs} = 12$) and ISO with AIP ($n_{cells} = 9$; $N_{pigs} = 4$). ***$P < 0.001$.

Repetitive activation of RyRs is restricted to coupled RyRs and mediated by CaMKII

At the cellular level, Ca^{2+} waves (i.e. propagating spontaneous Ca^{2+} release) contribute to potential arrhythmogenic activity due to activation of the NCX current. The likelihood of inducing Ca^{2+} waves depends on the simultaneous activation of multiple RyR clusters in close proximity. Thus, a higher number of sparks arising from the same RyR cluster, and/or a higher number of firing RyR clusters in close proximity, can increase the likelihood of wave initiation. We examined the spark activity of repetitively firing RyRs and how such activity is altered during β-adrenergic stimulation. RyR clusters were categorized as repetitive firing sites when at least two sparks occurred within 15 s of spark recording (Fig. 4*A*).

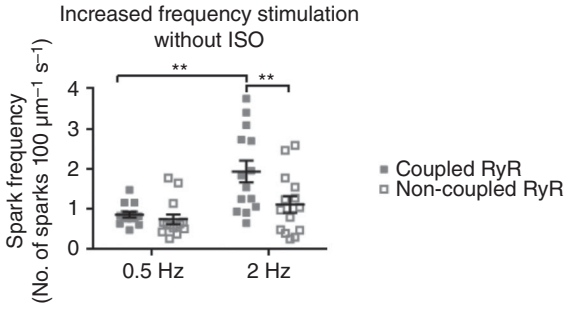

Figure 2. Specific modulation of coupled RyRs during high-frequency stimulation in the absence of ISO
Spark frequency in coupled and non-coupled RyRs during high-frequency stimulation in the absence of ISO ($n_{cells} = 15$; $N_{pigs} = 5$). $^{**}P < 0.01$.

At baseline, sparks originating from repetitive firing sites were equally prevalent in coupled *versus* non-coupled RyRs (Fig. 4*Ba*). In the presence of ISO, sparks from repetitive sites significantly increased for both coupled and non-coupled RyRs. However, the effects were more pronounced for coupled RyRs, with a tripling of the spark frequency compared to a doubling of the spark frequency at non-coupled regions (Fig. 4*Ba*). One potential cause of this increased spark frequency is the recruitment of new repetitive sites (Fig. 4*Bb*). These results mirrored those of the spark frequency analysis; at baseline, there were no obvious differences between coupled and non-coupled RyRs, whereas ISO treatment more than doubled the number of repetitive sites at coupled areas.

We further tested the role of CaMKII in control of Ca^{2+} sparks using AIP. The presence of AIP abolished the majority of the ISO-induced increases in spark frequency at coupled sites alone, without noticeably affecting non-coupled ones (Fig. 4*Ca*). Likewise, AIP reduced the recruitment of repetitive sites at coupled areas alone (Fig. 4*Cb*).

Mechanisms of CaMKII activation at coupled RyRs

Activation of CaMKII could be indirect through high local $[Ca^{2+}]_i$ or through other signalling pathways. Recent studies have described a β-adrenergic signalling cascade where CaMKII activation occurs via an NO-dependent pathway (Gutierrez *et al.* 2013; Curran *et al.* 2014). This was tested using the nitric oxide synthase 1 (NOS1) inhibitor L-VNIO (Fig. 5*A*). L-VNIO significantly reduced spark frequency in coupled RyRs but had no effect on non-coupled RyRs in the presence of ISO. Furthermore,

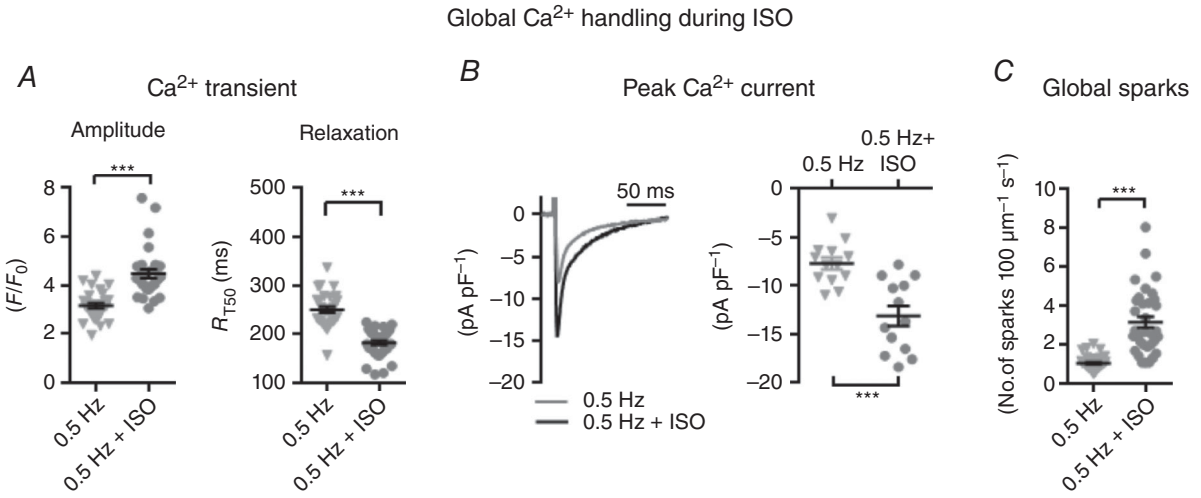

Figure 3. Increase in global Ca^{2+} handling during β-adrenergic stimulation
A, Ca^{2+} transient kinetics ($n_{cells} = 30$; $N_{pigs} = 9$); *B*, peak Ca^{2+} current amplitude ($n_{cells} = 13$; $N_{pigs} = 3$); and *C*, global spark frequency before and after ISO ($n_{cells} = 34$; $N_{pigs} = 11$). $^{***}P < 0.001$.

similar to the results obtained using AIP, SR Ca^{2+} content was not affected by L-VNIO application.

Epac, a direct target for cAMP, has also been reported to increase CaMKII activation independently of PKA (Pereira *et al.* 2013; Ruiz-Hurtado *et al.* 2013). To test this, we used the recently described Epac1 inhibitor CE3F4 (Courilleau *et al.* 2013) and Epac2 inhibitor ESI-05 (Domínguez-Rodríguez *et al.* 2015) (Fig. 5*B*). CE3F4 and ESI-05 did not affect spark frequency in either coupled or non-coupled RyRs under ISO stimulation. Similarly, the SR Ca^{2+} content was not altered by these agents.

Finally, we examined the role of local increases in $[Ca^{2+}]_i$ during the stimulation train (Fig. 5*C*). We indirectly estimated differences in local $[Ca^{2+}]_i$ by measuring the rate of upstroke of local Ca^{2+} transients at selected coupled and non-coupled regions. The rate of upstroke may be more indicative of local transient elevations of $[Ca^{2+}]_i$ than its amplitude in the same region. Despite a large increase in the local Ca^{2+} transient amplitude in non-coupled RyRs, the rate of upstroke at those areas remained substantially below that of coupled regions. These data therefore indicated that increases in the local $[Ca^{2+}]_i$ are far more pronounced at coupled than non-coupled areas, and are consistent with a much greater CaMKII activation at coupled RyR clusters.

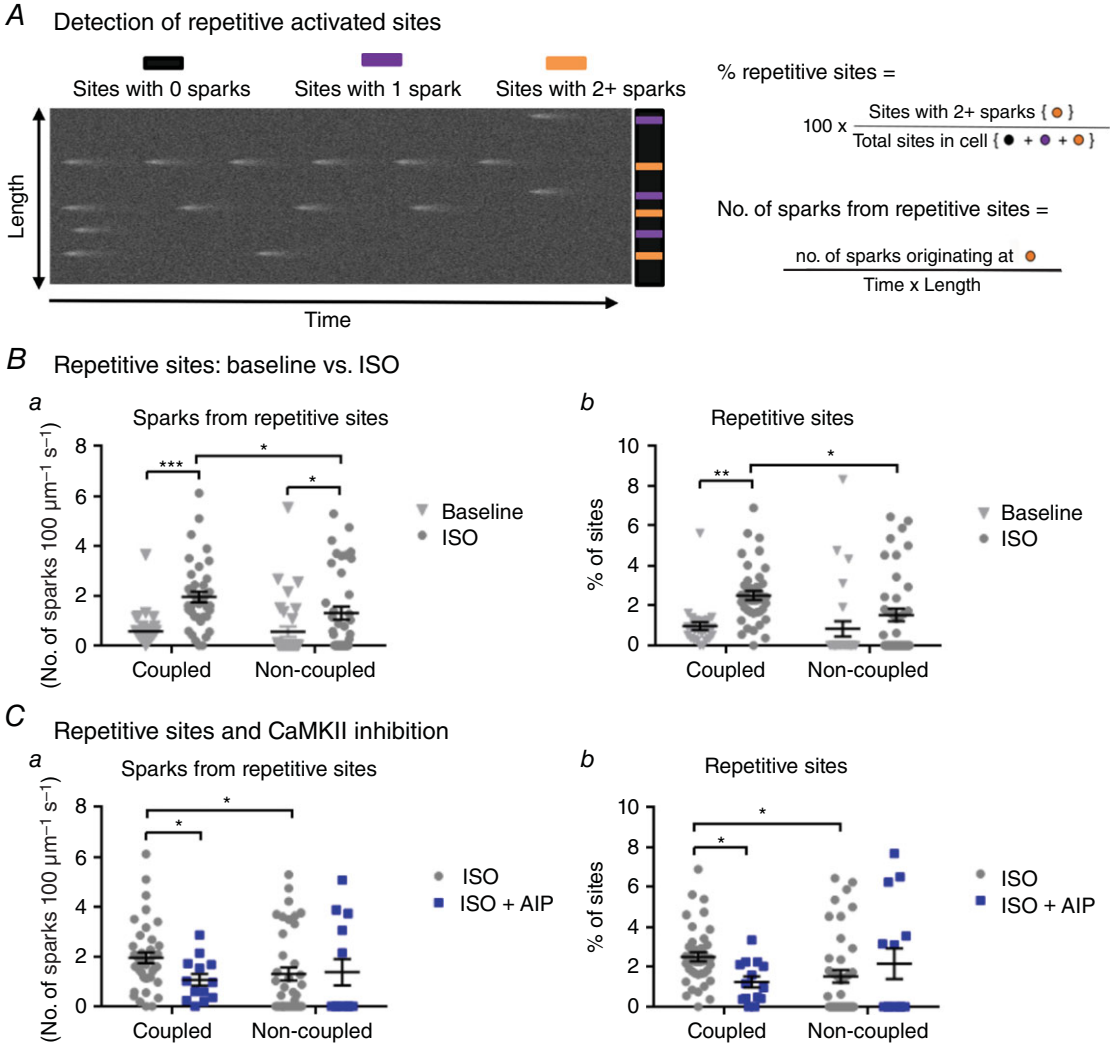

Figure 4. The activation of repetitive firing sites during ISO is higher in coupled areas and is regulated by CaMKII

A, left: theoretical example of a confocal line scan with non-active sites (black), sites with 1 spark (purple) and sites with 2 or more sparks (orange). Right: formulas used to determine the percentage of repetitive sites recruited and the spark frequency from repetitive firing sites. Both parameters are separately analysed for coupled and non-coupled RyRs. *B*, spark frequency and percentage of repetitive sites in coupled or non-coupled regions before ($n_{cells} = 27$; $N_{pigs} = 11$) and after ISO ($n_{cells} = 40$; $N_{pigs} = 16$). *C*, the spark frequency and percentage of repetitive release sites in coupled and non-coupled sites with ISO *vs.* ISO with AIP ($n_{cells} = 16$; $N_{pigs} = 5$). $^*P < 0.05$; $^{**}P < 0.01$; $^{***}P < 0.001$.

Taken together, these data indicate that the activation of CaMKII in coupled RyRs is likely to occur via local Ca^{2+} and NOS1 microdomains, and is not dependent on Epac.

CaMKII is equally distributed but has a higher level of phosphorylation in coupled sites

We previously showed an equal distribution of CaMKII in both coupled and non-coupled RyRs (Dries *et al.* 2013). However, the above results suggest a greater CaMKII activation near coupled RyRs after ISO stimulation. Therefore, we investigated whether there is an increased distribution of activated CaMKII [phospho-CaMKII Th286 (P-CaMKII)] in coupled RyRs when myocytes are conditioned at 0.5 Hz stimulation in the presence of ISO. Triple immunolabelling for RyR, NCX and P-CaMKII were performed and the fluorescence intensity for P-CaMKII was measured in the presence and absence of ISO in electrically paced myocytes (Fig. 6*A*). The total fluorescence intensity of P-CaMKII was not changed after ISO (Fig. 6*Ba*). However, local analysis of the fluorescence intensity in coupled relative to non-coupled RyRs within

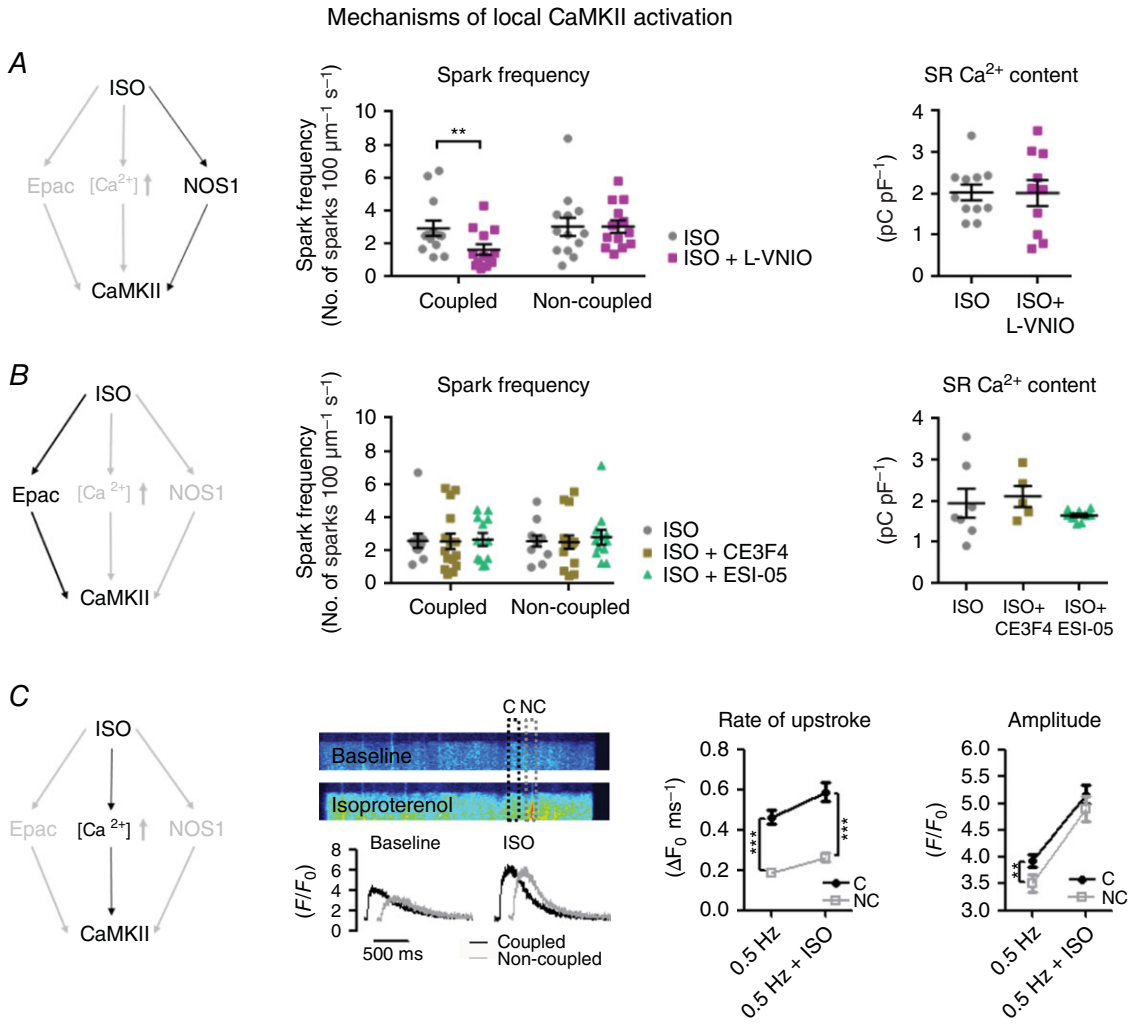

Figure 5. Activation of CaMKII is likely to occur via Ca^{2+} and NOS1 and is not dependent on Epac during β-adrenergic stimulation
A, the role of NOS1 in CaMKII activation after ISO stimulation. The effect of L-VNIO on Ca^{2+} spark frequency in coupled and non-coupled RyRs ($n_{cells} = 13$; $N_{pigs} = 3$) and on SR Ca^{2+} content in the presence of ISO ($n_{cells} = 10$; $N_{pigs} = 3$). *B*, the role of Epac in CaMKII activation after ISO stimulation. The effect of CE3F4 (Epac1; $n_{cells} = 15$; $N_{pigs} = 3$) and ESI-05 (Epac2; $n_{cells} = 12$; $N_{pigs} = 3$) on Ca^{2+} spark frequency in coupled and non-coupled RyRs and on SR Ca^{2+} content (CE3F4: $n_{cells} = 5$; $N_{pigs} = 3$; ESI-05: $n_{cells} = 11$; $N_{pigs} = 3$) in the presence of ISO. *C*, the role of changes in $[Ca^{2+}]_i$ in CaMKII activation after ISO stimulation. Example of a confocal line scan image with a coupled and non-coupled region selected and corresponding local Ca^{2+} transient plots normalized to the diastolic $[Ca^{2+}]_i$ (please note that traces have been slightly shifted along the x-axis for clarity). The rate of upstroke and Ca^{2+} transient amplitude in coupled and non-coupled regions in the absence and presence of ISO ($n_{cells} = 30$; $N_{pigs} = 10$). $^{**}P < 0.01$; $^{***}P < 0.001$.

each myocyte revealed a higher P-CaMKII in coupled RyRs (Fig. 6*Bb*). These data confirm our findings at the functional level, further supporting the hypothesis of a local CaMKII activation near coupled RyRs.

PKA modulates spark frequency in both coupled and non-coupled RyRs, at least partially by modulating SR Ca^{2+} load

Our mechanistic dissection uncovered that coupled RyRs are differentially regulated by ISO, in particular via local CaMKII activation, which is dependent on high local $[Ca^{2+}]_i$ and NOS1. Furthermore, CaMKII-dependent modulation occurred in the absence of changes in SR Ca^{2+} content. These insights leave a number of questions unanswered: how is spark frequency increased by ISO at non-coupled clusters and what is the role of PKA?; and to what extent does SR load influence spark activity at coupled and non-coupled areas compared to RyR phosphorylation? We therefore first examined how PKA modulates coupled and non-coupled RyRs. Application of the peptide-based PKA inhibitor PKI during β-adrenergic stimulation reduced the frequency of sparks arising from both coupled and non-coupled RyRs (Fig. 7*A*) and reduced the SR Ca^{2+} content (Fig. 7*B*). Analysis of the relationship between SR Ca^{2+} content and spark frequency indicated that the reduced activity of coupled and non-coupled RyRs by PKA occurred together with a reduction in SR Ca^{2+} content (Fig. 7*C*). These experiments were repeated with another PKA inhibitor, H-89, and similar results were obtained (Fig. 8). Therefore, it is possible that the observed RyR modulation depends on both direct RyR modifications (i.e. phosphorylation) and indirect regulation via changes in SR Ca^{2+} load.

To distinguish between a direct effect of PKA on RyR and an effect on store load, Ca^{2+} sparks were recorded after reducing SR Ca^{2+} load in the presence of ISO (Fig. 9*Aa*). To this end, we conditioned cells as described before and applied a short caffeine pulse (400 ms, 10 mM caffeine) 6 s before the last Ca^{2+} transient to induce (partial) emptying of the SR before spark recording. The timing and duration of the caffeine pulse ensured an RyR activity that was not modified by caffeine at the time of spark collection. Additionally, the time to 50% relaxation of the last Ca^{2+} transient prior to spark recording was not different from the Ca^{2+} transient prior to caffeine application (data not shown), indicating that this intervention did not affect PLN phosphorylation. The intervention did, however, reduce SR Ca^{2+} content as assessed in Fig. 9*Ab*.

The lower SR Ca^{2+} load was associated with a reduction in the Ca^{2+} spark frequency for both coupled and non-coupled RyRs (Fig. 9*B* and Fig. 9*C*, light blue symbols, compared to ISO alone in light grey symbols). However, spark frequency remained higher when compared to the baseline spark frequency with an equal SR Ca^{2+} load (light blue *vs.* black in Fig. 9*C*). These findings indicate that the increase in SR Ca^{2+} load only partially

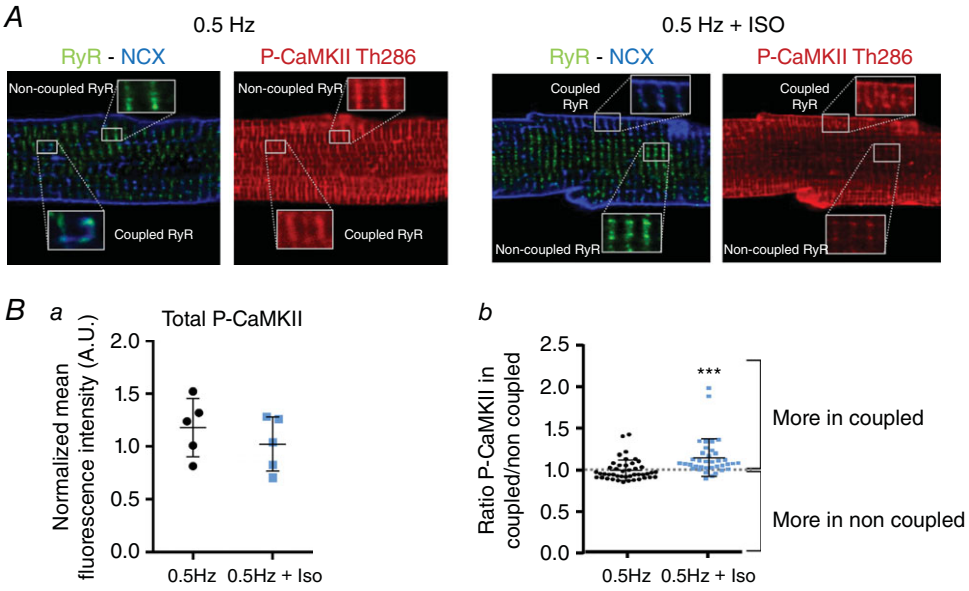

Figure 6. Distribution of P-CaMKII in coupled and non-coupled RyRs
A, example of triple immunostaining of myocytes in the presence and absence of ISO. RyRs are stained in green, NCX in blue and P-CaMKII in red. Higher magnification images of the indicated regions are shown for coupled and non-coupled RyRs. *Ba*, total fluorescence intensity for P-CaMKII in the absence and presence of ISO; *b*, the ratio of fluorescence intensity for P-CaMKII in coupled and non-coupled RyRs in the absence and presence of ISO (n_{cells} = 7–10 cells per pig; N_{pigs} = 5). *** $P < 0.001$.

accounts for the response of coupled and non-coupled RyRs to β-adrenergic stimulation. In addition, similar experiments in which the SR Ca^{2+} load was reduced were also performed in the presence of AIP. Here lowering of SR Ca^{2+} load resulted in significant reduction of spark frequency in non-coupled RyRs but the low frequency in coupled RyRs was not further reduced, supporting the importance of the regulation of coupled RyRs via CaMKII (Fig. 9*C*, green symbols compared to dark blue symbols).

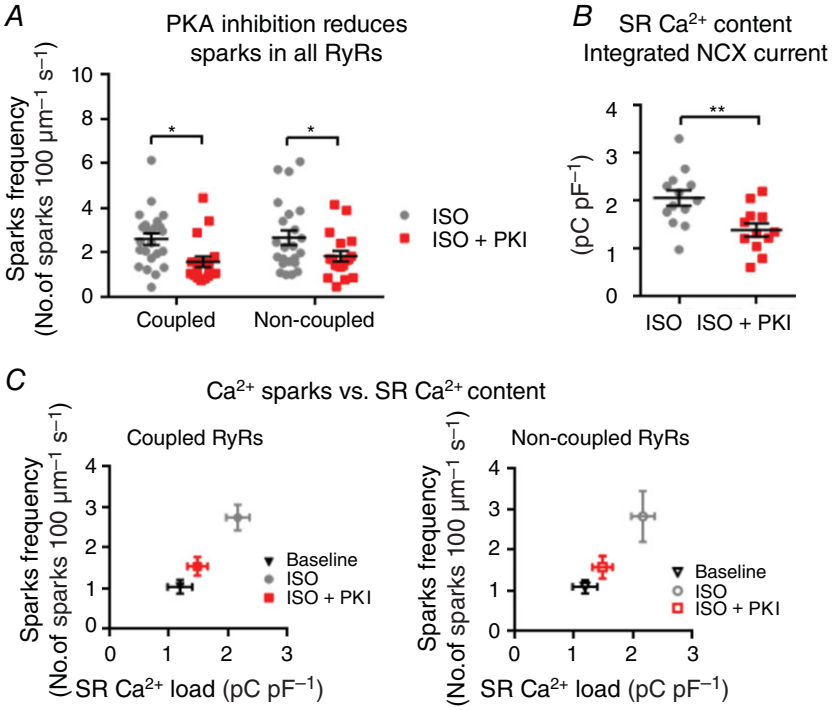

Figure 7. PKA affects coupled and non-coupled RyRs during β-adrenergic stimulation
A, the effect of PKI on Ca^{2+} spark frequency in coupled and non-coupled RyRs after ISO ($n_{cells} = 18$; $N_{pigs} = 5$). *B*, the effect of PKI on the SR Ca^{2+} content after ISO ($n_{cells} = 12$; $N_{pigs} = 4$). *C*, the relationship between SR Ca^{2+} load and Ca^{2+} spark frequency at baseline ($n_{cells} = 7$; $N_{pigs} = 6$), with ISO ($n_{cells} = 10$; $N_{pigs} = 8$) and with ISO plus PKI ($n_{cells} = 8$; $N_{pigs} = 3$). $^{*}P < 0.05$; $^{**}P < 0.01$.

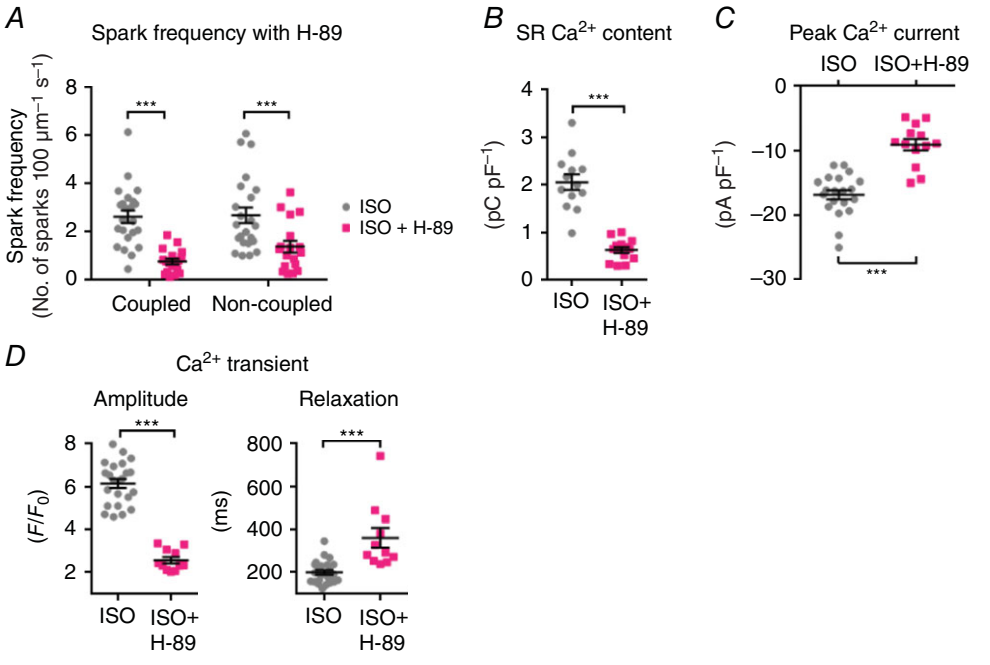

Figure 8. H-89 affects all RyRs and global Ca^{2+} handling during β-adrenergic stimulation
A, the effect of H-89 on Ca^{2+} spark frequency in coupled and non-coupled RyRs after ISO ($n_{cells} = 18$; $N_{pigs} = 4$). *B*, the effect of H-89 on the SR Ca^{2+} content ($n_{cells} = 14$; $N_{pigs} = 4$); *C*, peak Ca^{2+} current ($n_{cells} = 13$; $N_{pigs} = 3$); and *D*, Ca^{2+} transient kinetics ($n_{cells} = 11$; $N_{pigs} = 4$). *** $P < 0.001$.

CaMKII- and PKA-dependent effects on global Ca^{2+} transients triggered by LTCC

We have focused thus far on the spontaneous release events at resting membrane potential and on the SR Ca^{2+} content. We next examined the contribution of CaMKII activation in the dyadic cleft on Ca^{2+} handling during depolarizing pulses.

As illustrated in Fig. 10*Aa*, the increase in I_{CaL} under ISO is sensitive to CaMKII inhibition. Despite this reduction of ICaL, global Ca^{2+} transients are not significantly affected in amplitude or kinetics of upstroke or relaxation (Fig. 10*Ab*). A possible factor here is that the SR Ca^{2+} load was not reduced by CaMKII inhibition as shown before in Fig. 1*Bb* and may be related to lack of an appreciable effect on SERCA activity; this observation is supported by the maintained high rate of relaxation. Nevertheless, the effect of CaMKII inhibition on I_{CaL} and coupled RyRs P_o can be detected in the rate of upstroke of I_{CaL}-triggered local Ca^{2+} transients in the dyadic cleft (Fig. 10*Ac*).

In contrast, as illustrated in Fig. 10*Ba*, PKI not only reduced I_{CaL} but also had a major effect on the global Ca^{2+} transient, reducing the amplitude and kinetics of upstroke and rate of decay (Fig. 10*Bb*). This is probably due to a major reduction in SR Ca^{2+} content (Fig. 7*B*), and concordant with a reduced SERCA activity, evidenced by the slowing of relaxation with PKI.

These results indicate that β-adrenergic activation of CaMKII has effects that are spatially restricted to the dyadic cleft. In contrast, PKA has global effects on systolic Ca^{2+} handling and Ca^{2+} transient amplitude during β-adrenergic stimulation, at least partly indirectly, via alterations in SR load.

Discussion

The present data show that different signalling microdomains underlie the integrated response to β-adrenergic modulation of LTCCs, PLN and RyRs. CaMKII activation

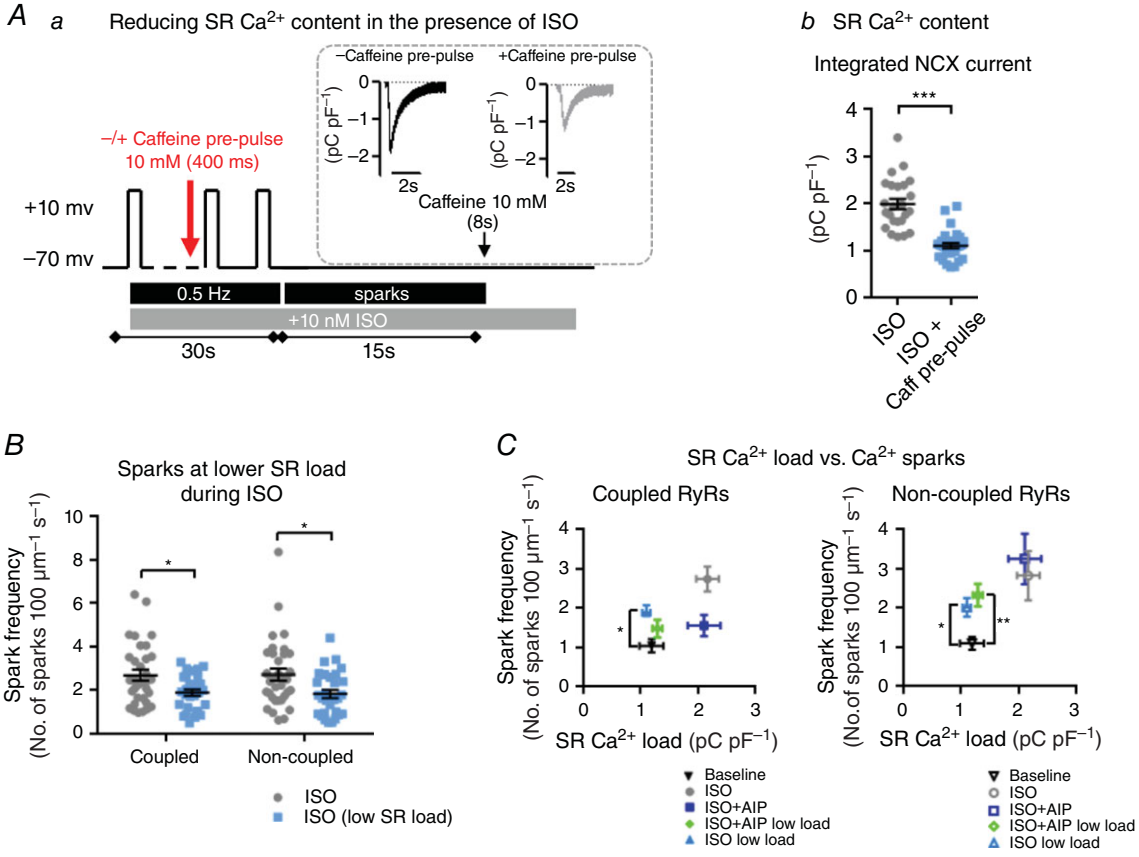

Figure 9. A reduced SR Ca^{2+} load affects both coupled and non-coupled RyRs during maintained β-adrenergic stimulation
Aa, myocytes are stimulated in the presence of ISO as described before. To reduce the SR Ca^{2+} load, a brief caffeine pulse (400 ms) is applied before the end of the stimulation train. *Ab*, SR Ca^{2+} content; and *B*, spark frequency in the presence of ISO or ISO with a reduced SR Ca^{2+} load ($n_{cells} = 24$; $N_{pigs} = 3$). *C*, the relationship between SR Ca^{2+} load and Ca^{2+} spark frequency at baseline, ISO ($n_{cells} = 10$; $N_{pigs} = 8$), ISO with low SR load ($n_{cells} = 25$; $N_{pigs} = 3$), and AIP and AIP with low SR load ($n_{cells} = 11$; $N_{pigs} = 4$) in coupled and non-coupled RyRs. $^*P < 0.05$; $^{***}P < 0.001$.

is confined to the dyadic cleft, where it enhances the P_o of RyRs and LTCCs and contributes to the increase of the local Ca^{2+} release and diastolic events. Enhanced SR Ca^{2+} uptake and SR Ca^{2+} load are PKA-dependent and major determinants of the global increase of Ca^{2+} cycling.

The dyadic cleft is a microdomain for CaMKII and NOS1-dependent modulation of RyRs

During β-adrenergic stimulation, CaMKII-dependent modulation of RyRs exclusively occurs in the restricted area of the dyadic cleft. These data are in line with our previous report of CaMKII activation during high-frequency stimulation in the absence of ISO (Dries *et al.* 2013). NOS1 equally participates in the local modulation of coupled RyRs. However, the current data cannot identify the relationship between CaMKII and NOS1 because inhibition of either pathway reduces spark frequency to baseline levels. This is consistent with a sequential and interdependent activation, but the current data cannot inform about the hierarchy of this dyad-specific signalling.

NOS1 could enhance RyR activity directly through nitrosylation or indirectly via nitrosylation of CaMKII, or both. Data obtained in rabbit myocytes (Curran *et al.* 2014) suggest that CaMKII is activated downstream of NO. These authors show that after pre-incubation of purified CaMKII with Ca^{2+} and CaM, application of SNAP (NO donor) resulted in a high CaMKII activity. This was not observed when pre-incubated with EGTA, indicating that high levels of Ca^{2+} are a prerequisite for CaMKII activation by NO. Erickson *et al.* (2015) recently reported that NO treatment after Ca^{2+}/CaM binding can result in the autonomous activation of CaMKII via S-nitrosylation. This CaMKII activation mechanism was suggested earlier by Guttierez *et al.* (2013) who furthermore showed that CaMKII was activated independently of $[Ca^{2+}]_i$ when ISO was applied in quiescent cells. It should be noted, however, that previous studies used high ISO concentrations, 1 μM

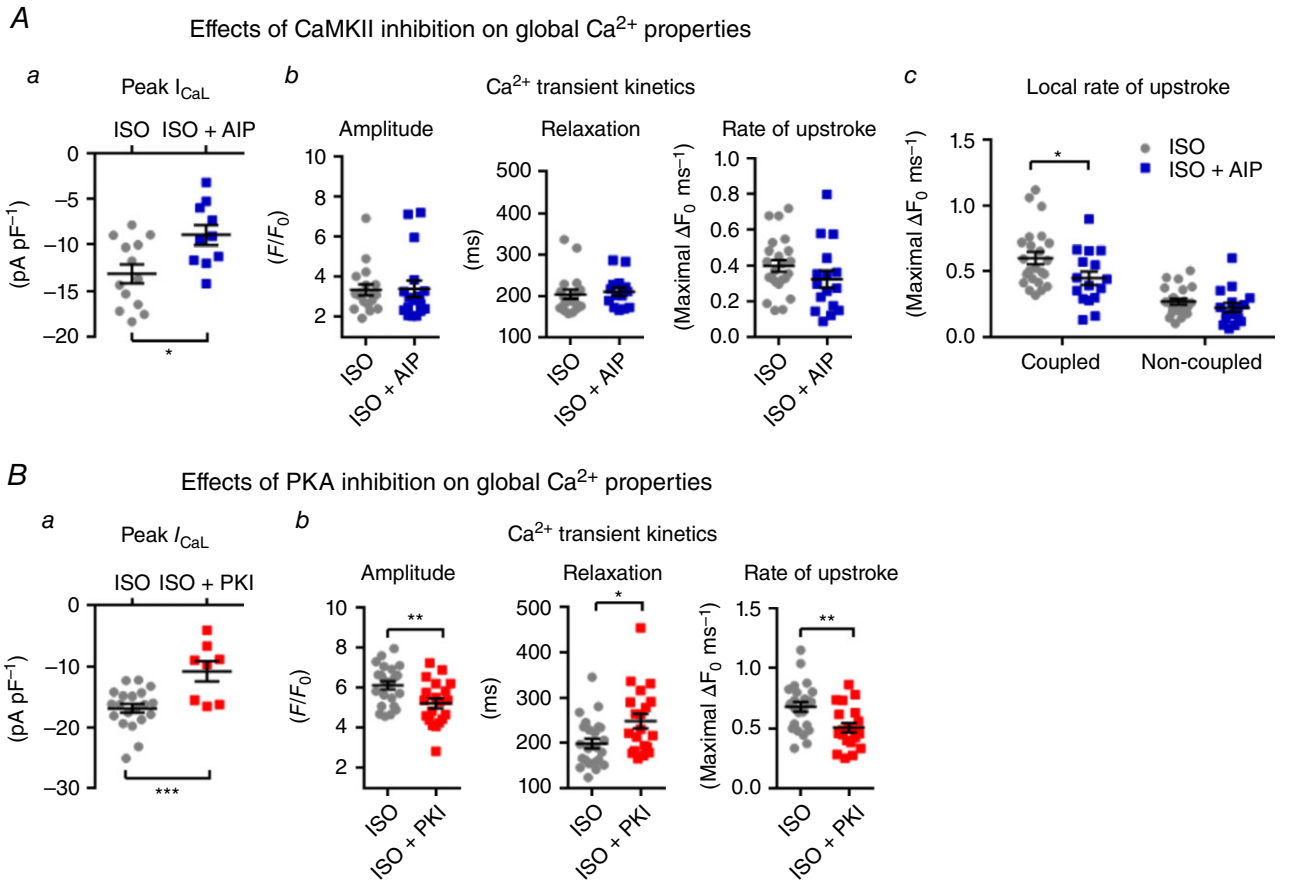

Figure 10. Global Ca^{2+} handling is increased during β-adrenergic stimulation via global PKA effects and local CaMKII effects
Aa, peak Ca^{2+} current amplitude ($n_{cells} = 10$; $N_{pigs} = 3$); and *b*, global and c, local Ca^{2+} transient kinetics in the presence of ISO or ISO with AIP ($n_{cells} = 14$; $N_{pigs} = 4$). *Ba*, peak Ca^{2+} current amplitude ($n_{cells} = 8$; $N_{pigs} = 3$); and *b*, global Ca^{2+} transient kinetics in the presence of ISO or ISO with PKI ($n_{cells} = 20$; $N_{pigs} = 5$). $^*P < 0.05$; $^{**}P < 0.01$; $^{***}P < 0.001$.

(Gutierrez *et al.* 2013) and 250 nM (Curran *et al.* 2014) as opposed to 10 nM used in this study.

If NOS1 is the primary step in leading to RyR phosphorylation, little is known regarding how β-AR could activate NOS1. NOS1, RyRs and CaMKII are spatially colocalized (Barouch *et al.* 2002; Bendall *et al.* 2004; Damy *et al.* 2004) and this could create a local NO microdomain near coupled RyRs. Recently, Curran *et al.* (2014) proposed a role for β1-AR and NOS1 activation via AKT signalling. However, the exact mechanism of NOS1 activation upon β-adrenergic signalling remains elusive.

Although data in the present study are compatible with a NOS1 activation of CaMKII, the data also suggest that direct activation of CaMKII by Ca^{2+} is involved in RyR regulation. Indeed, CaMKII activation required the increased Ca^{2+} levels associated with the conditioning pulses (which are PKA-dependent): when the amplitudes of the Ca^{2+} transients during the conditioning pulses were reduced with PKI (Fig. 10*B*), the activity of coupled receptors also decreased. While this could imply co-activation of PKA and CaMKII, reducing the SR Ca^{2+} load, even without reducing PKA activity (Fig. 9*C*), also reduced sparks in coupled sites, suggesting again that the CaMKII activation is dependent on local Ca^{2+}. The local Ca^{2+} levels in the dyadic cleft during depolarizing pulses are indeed much higher than in the global cytosol (e.g. Acsai *et al.* 2011 in a similar myocyte cell type) and analysis of the local Ca^{2+} transients during the conditioning pulses is consistent with a different local $[Ca^{2+}]_i$ between coupled and non-coupled RyRs (Fig. 5*C*).

Another pathway for CaMKII activation is through reactive oxygen species (ROS). So far there is no conclusive evidence indicating that ROS production during β-adrenergic stimulation can directly activate CaMKII. NO-dependent CaMKII modulation has been reported to occur independently of ROS, as direct ROS scavenging during β-adrenergic stimulation did not affect SR Ca^{2+} sparks (Gutierrez *et al.* 2013) and NOX2 inhibition during ISO did not shift the SR load–leak relationship (Curran *et al.* 2014). In line with these studies, global ROS scavenging using NAC did not affect the spark frequency in coupled or non-coupled sites, nor did it affect SR Ca^{2+} content (Fig. 11). Likewise, Bovo *et al.* (2012, 2015) showed an increased ROS production during β-adrenergic stimulation but it was only the direct oxidation of RyRs that changed RyR sensitivity. On the other hand, we recently showed that enhanced RyR activity at coupled sites during high-frequency stimulation depends on the interdependent activation of NOX2 and CaMKII (Dries *et al.* 2013), these data being consistent with a ROS microdomain in the dyadic cleft that may regulate CaMKII activity.

In the present study, local CaMKII activation at coupled sites occurred independently from Epac. These data are in line with the study of Curran *et al.* (2014), where neither direct activation of Epac nor increases in cAMP altered the SR Ca^{2+} load–leak relationship. Epac activation was also not able to alter the spark frequency. Others, however, found a clear link between Epac activation and an increased SR Ca^{2+} leak via CaMKII-dependent phosphorylation of RyR-S2814 (Pereira *et al.*, 2007, 2013). Pereira *et al.* (2015) recently showed that in different subcellular regions specific Epac isoforms are present, with Epac2 located near TTs and involved in the regulation of SR Ca^{2+} leak. The difference of the aforementioned study with the present data may be a species-dependent difference. In addition, the specificity of both Epac inhibitors could not be assessed in the present study.

Lastly, the signalling to CaMKII could be related to local β-AR subtypes. In rat myocytes β2-ARs have been shown to preferentially reside within TTs in contrast to the β1-ARs, which are located across the entire cell surface and may be expected to mediate a more 'global' response compared to β2-ARs (Nikolaev *et al.* 2010).

Integrated CaMKII and PKA signalling during β-adrenergic stimulation

CaMKII and PKA pathways both contribute to the β-adrenergic response. CaMKII signalling appears to have its major effects on diastolic events with more modest impact on systolic function, whereas PKA has major impact on systolic function through the modulation of SR Ca^{2+} content.

While this opens interesting perspectives as discussed in the next section, there are also several unanswered questions about the interaction and relative importance of the two pathways in modulating RyR activity.

A simultaneous requirement of CaMKII and PKA for the enhancement of RyR activity has recently been proposed by Polakova *et al.* (2015), using mouse myocytes,

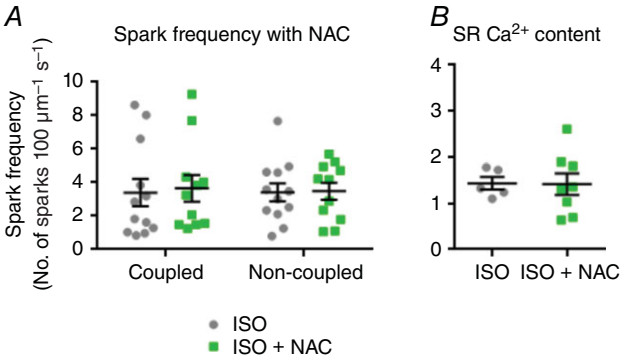

Figure 11. Global ROS scavenging does not affect RyRs and SR Ca^{2+} content during β-adrenergic stimulation
A, the effect of NAC on Ca^{2+} spark frequency in coupled and non-coupled RyRs after ISO ($n_{cells} = 11$; $N_{pigs} = 3$); and *B*, on the SR Ca^{2+} content ($n_{cells} = 8$; $N_{pigs} = 3$).

where presumably all RyRs are coupled. If we only consider coupled RyRs, the conclusions of Polakova are consistent with the present data (Fig. 7) showing that PKA inhibition reduces activity of coupled RyRs. A specific explanation here is, as stated above, that PKI inhibition reduces cellular Ca^{2+} levels (because it lowers the SR Ca^{2+} load) and thereby prevents CaMKII activation. Nevertheless, with the reduced Ca^{2+} load in the presence of PKA, sparks from coupled RyRs were still elevated and sensitive to CaMKII inhibition. An alternative explanation may therefore be that PKA has a direct co-activating effect.

Not much is known about such a potential molecular mechanism. The role of PKA-dependent phosphorylation at S2808/2809 in itself and in contrast to S2814 has been debated (Wehrens *et al.* 2004; Xiao *et al.*, 2006, 2007; MacDonnell *et al.* 2008; Morimoto *et al.* 2009; Shan *et al.* 2010). Molecular modelling found even more phosphorylation sites on RyR2 (Van Petegem, 2012) but their relative functional roles remain largely unknown.

A

Ca^{2+} waves induced at 2 Hz frequency with ISO

ISO

	waves	no waves	
Coupled	16	17	33
Non-coupled	6	27	33
Total	22	44	66

ISO + AIP

	waves	no waves	
Coupled	11	9	20
Non-coupled	8	12	20
Total	19	21	40

B

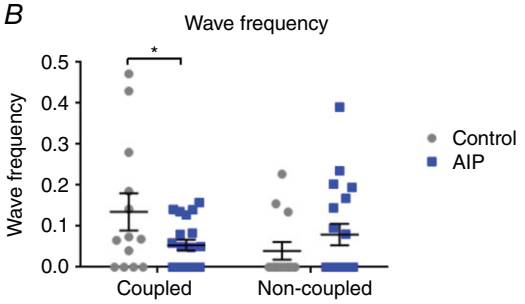

Figure 12. More Ca^{2+} waves originate from coupled RyRs after ISO
A, incidence of Ca^{2+} waves occurring in coupled *vs.* non-coupled RyRs when stimulating cells at high frequency (2 Hz) and in the presence of ISO ($n_{cells} = 33$; $N_{pigs} = 8$) and ISO with AIP ($n_{cells} = 20$; $N_{pigs} = 3$). *B*, preliminary data set showing the Ca^{2+} waves frequency in coupled *vs.* non-coupled RyRs in the presence of AIP ($n_{cells} = 20$; $N_{pigs} = 3$). $^*P < 0.05$.

Our initial hypothesis was for a dual phosphorylation of coupled RyRs at dyadic sites with cumulated stimulating effects and highest spark frequency for coupled RyRs (PKA and CaMKII) compared to non-coupled RyRs (PKA only). However, the data presented in this study do not show additive effects at coupled sites despite the fact that there is a site-specific CaMKII effect.

The most puzzling aspect to our data is why inhibition of CaMKII results in lower spark frequency in coupled RyRs *vs.* non-coupled RyRs despite maintained PKA activation. If the role of PKA is predominantly through increased SR Ca^{2+} load, there should not be a difference between coupled and non-coupled RyRs, assuming SR Ca^{2+} load is the same throughout the SR network. We have previously investigated whether there were standing SR gradients after stopping the conditioning pulses and at the time of sparks recording, but could not detect any (Dries *et al.* 2013). The remaining explanation, and hypothesis, is then that PKA modulation of RyRs at coupled sites is less predominant than at non-coupled sites. Differences in AKAP could also play a role and explain the differential contribution of PKA but are presently beyond study.

Finally, the data from Fig. 9*C* suggest that there is a load-independent effect of PKA presumably through phosphorylation of RyR clusters.

Limitations

A number of potential mechanisms were not further investigated, some due to methodological limitations. We failed to find suitable NOS1 antibodies to work in the pig. So far we also have not been able to measure spatially confined signals through ROS, because of low signals. Immunostaining is not optimal for quantification of P-CaMKII, although the signals appear to be quite specific (supported by KN-93 inhibition of immunostaining – pilot data, not shown) but measuring localized CaMKII signals in living cells requires fluorescence resonance energy transfer probes that can only be introduced during cell culture (Erickson *et al.* 2011).

There are additional hypotheses regarding micro-domain signalling for future studies. These include the distribution of β-ARs (Nikolaev *et al.* 2010) as well as the macrocomplex properties of the RyR clusters, coupled *vs.* non-coupled. So far biochemical approaches are not feasible due to the difficulties in extracting the two RyR populations but we are currently developing methods for *in situ* characterization.

In the present study we could not resolve differences in the total level of CaMKII phosphorylation despite the fact that the functional evidence clearly indicates CaMKII-dependent phosphorylation at coupled sites, which make up about 50% of all sites. Several factors may contribute to this. The data in Fig. 6 suggest there is a base-line degree of phosphorylation of CaMKII. Against this

background small changes may be difficult to detect. For the data on total P-CaMKII, we also compare populations of cells, introducing more variability and the inherent variability of the assay decreases the ability to detect small changes in fluorescence between cells. In our analysis, a ratio of staining in coupled *vs.* non-coupled RyRs within each cell is determined on a cell by cell basis and reduces noise on these measurements. Furthermore, we applied only a low concentration of ISO to avoid massive stimulation and Ca^{2+} overload, which probably resulted in submaximal activation of CaMKII.

Perspectives and conclusions

The increase in diastolic events with β-adrenergic stimulation, at the level of the whole cell, is both PKA- and CaMKII-driven. Yet, the sparks that are specifically CaMKII-dependent, i.e. at coupled sites, probably have the highest potential for triggering Ca^{2+} wave activity and deleterious membrane depolarizations. First, as shown in Fig. 4 these are the sites that have more repetitive sparks and CaMKII increases the number of coupled sites being recruited for repetitive activation, thereby facilitating summation in space and time to form propagating Ca^{2+} waves. Secondly, the location at the membrane promotes direct activation of the NCX current. Lastly, *in vivo* β-adrenergic stimulation is a combination of increased frequency (chronotropy at the SA node) and direct β-AR-mediated effects as studied here at low frequency. As we have previously shown that frequency by itself specifically enhances diastolic events at coupled RyRs (Dries *et al.* 2013), these two mechanisms are likely to reinforce each other and predict wave formation from coupled RyRs. Data on Ca^{2+} waves using myocytes conditioned at a high frequency in the presence of ISO support this concept: more Ca^{2+} waves originated at coupled RyRs than at non-coupled RyRs (Fig. 12*A*). A preliminary data set further shows that this phenomenon is under control of CaMKII, as inhibition with AIP decreased Ca^{2+} wave frequency at coupled sites only (Fig. 12*B*).

The present results also indicate that CaMKII activation has limited impact on the global Ca^{2+} handling that underlies the positive inotropic and lusitropic actions of β-adrenergic stimulation. Therefore, the present data further support the concept that CaMKII may be a preferential target for reducing arrhythmic events as inhibition would have minor effects on contraction and relaxation.

Finally, although the current study has concentrated on ventricular myocytes, there is also the possibility that similar RyR subpopulation modulation is present in other cell types. Previous work has shown the presence of a large fraction of non-coupled RyRs in atrial cells of large mammals including humans (Dibb *et al.* 2009; Lenaerts *et al.* 2009). Whether these RyR subpopulations have different modulation is the subject of ongoing work.

In conclusion, the present data extend the concept of microdomain signalling in the dyadic cleft and open perspectives for selective modulation of subpopulations of RyRs.

References

Acsai K, Antoons G, Livshitz L, Rudy Y & Sipido KR (2011). Microdomain [Ca^{2+}] near ryanodine receptors as reported by L-type Ca^{2+} and Na^{+}/Ca^{2+} exchange currents. *J Physiol* **589**, 2569–2583.

Agarwal SR, Yang P-C, Rice M, Singer CA, Nikolaev VO, Lohse MJ, Clancy CE & Harvey RD (2014). Role of membrane microdomains in compartmentation of cAMP signalling. *PLoS ONE* **9**, e95835.

Barouch LA, Harrison RW, Skaf MW, Rosas GO, Cappola TP, Kobeissi ZA, Hobai IA, Lemmon CA, Burnett AL, O'Rourke B, Rodriguez ER, Huang PL, Lima JAC, Berkowitz DE & Hare JM (2002). Nitric oxide regulates the heart by spatial confinement of nitric oxide synthase isoforms. *Nature* **416**, 337–339.

Bendall JK, Damy T, Ratajczak P, Loyer X, Monceau V, Marty I, Milliez P, Robidel E, Marotte F, Samuel J-L & Heymes C (2004). Role of myocardial neuronal nitric oxide synthase–derived nitric oxide in β-adrenergic hyporesponsiveness after myocardial infarction–induced heart failure in rat. *Circulation* **110**, 2368–2375.

Bovo E, Lipsius SL & Zima AV (2012). Reactive oxygen species contribute to the development of arrhythmogenic Ca^{2+} waves during β-adrenergic receptor stimulation in rabbit cardiomyocytes. *J Physiol* **590**, 3291–3304.

Bovo E, Mazurek SR, de Tombe PP & Zima AV (2015). Increased energy demand during adrenergic receptor stimulation contributes to Ca^{2+} wave generation. *Biophys J* **109**, 1583–1591.

Courilleau D, Bouyssou P, Fischmeister R, Lezoualc'h F & Blondeau J-P (2013). The (R)-enantiomer of CE3F4 is a preferential inhibitor of human exchange protein directly activated by cyclic AMP isoform 1 (Epac1). *Biochem Biophys Res Commun* **440**, 443–448.

Curran J, Hinton MJ, Ríos E, Bers DM & Shannon TR (2007). β-Adrenergic enhancement of sarcoplasmic reticulum calcium leak in cardiac myocytes is mediated by calcium/calmodulin-dependent protein kinase. *Circ Res* **100**, 391–398.

Curran J, Tang L, Roof SR, Velmurugan S, Millard A, Shonts S, Wang H, Santiago D, Ahmad U, Perryman M, Bers DM, Mohler PJ, Ziolo MT & Shannon TR (2014). Nitric oxide-dependent activation of CaMKII increases diastolic sarcoplasmic reticulum calcium release in cardiac myocytes in response to adrenergic stimulation. *PLoS ONE* **9**, e87495.

Damy T, Ratajczak P, Shah AM, Camors E, Marty I, Hasenfuss G, Marotte F, Samuel J-L & Heymes C (2004). Increased neuronal nitric oxide synthase-derived NO production in the failing human heart. *Lancet* **363**, 1365–1367.

Dibb KM, Clarke JD, Horn MA, Richards MA, Graham HK, Eisner DA & Trafford AW (2009). Characterization of an extensive transverse tubular network in sheep atrial myocytes and its depletion in heart failure. *Circ Heart Fail* **2**, 482–489.

Domínguez-Rodríguez A, Ruiz-Hurtado G, Sabourin J, Gómez AM, Alvarez JL & Benitah J-P (2015). Proarrhythmic effect of sustained EPAC activation on TRPC3/4 in rat ventricular cardiomyocytes. *J Mol Cell Cardiol* **87**, 74–78.

Dries E, Bito V, Lenaerts I, Antoons G, Sipido KR & Macquaide N (2013). Selective modulation of coupled ryanodine receptors during microdomain activation of calcium/calmodulin-dependent kinase II in the dyadic cleft. *Circ Res* **113**, 1242–1252.

Erickson JR, Patel R, Ferguson A, Bossuyt J & Bers DM (2011). Fluorescence resonance energy transfer-based sensor Camui provides new insight into mechanisms of calcium/calmodulin-dependent protein kinase II activation in intact cardiomyocytes. *Circ Res* **109**, 729–738.

Erickson JR, Nichols CB, Uchinoumi H, Stein ML, Bossuyt J, Bers DM (2015). S-nitrosylation induces both autonomous activation and inhibition of calcium/calmodulin-dependent protein kinase II δ. *J Biol Chem* **290**, 25646–25656.

Ferrero P, Said M, Sánchez G, Vittone L, Valverde C, Donoso P, Mattiazzi A & Mundiña-Weilenmann C (2007). Ca^{2+}/calmodulin kinase II increases ryanodine binding and Ca^{2+}-induced sarcoplasmic reticulum Ca^{2+} release kinetics during β-adrenergic stimulation. *J Mol Cell Cardiol* **43**, 281–291.

Gorelik J, Wright PT, Lyon AR & Harding SE (2013). Spatial control of the βAR system in heart failure: the transverse tubule and beyond. *Cardiovasc Res* **98**, 216–224.

Gutierrez DA, Fernandez-Tenorio M, Ogrodnik J & Niggli E (2013). NO-dependent CaMKII activation during β-adrenergic stimulation of cardiac muscle. *Cardiovasc Res* **100**, 392–401.

Heinzel FR, Bito V, Volders PGA, Antoons G, Mubagwa K & Sipido KR (2002). Spatial and temporal inhomogeneities during Ca^{2+} release from the sarcoplasmic reticulum in pig ventricular myocytes. *Circ Res* **91**, 1023–1030.

Jayasinghe I, Crossman D, Soeller C & Cannell M (2012). Comparison of the organization of T-tubules, sarcoplasmic reticulum and ryanodine receptors in rat and human ventricular myocardium. *Clin Exp Pharmacol Physiol* **39**, 469–476.

Lenaerts I, Bito V, Heinzel FR, Driesen RB, Holemans P, D'hooge J, Heidbüchel H, Sipido KR & Willems R (2009). Ultrastructural and functional remodeling of the coupling between Ca^{2+} influx and sarcoplasmic reticulum Ca^{2+} release in right atrial myocytes from experimental persistent atrial fibrillation. *Circ Res* **105**, 876–885.

Leroy J, Abi-Gerges A, Nikolaev VO, Richter W, Lechêne P, Mazet J-L, Conti M, Fischmeister R & Vandecasteele G (2008). Spatiotemporal dynamics of β-adrenergic cAMP signals and L-type Ca^{2+} channel regulation in adult rat ventricular myocytes role of phosphodiesterases. *Circ Res* **102**, 1091–1100.

Louch WE, Bito V, Heinzel FR, Macianskiene R, Vanhaecke J, Flameng W, Mubagwa K & Sipido KR (2004). Reduced synchrony of Ca^{2+} release with loss of T-tubules – a comparison to Ca^{2+} release in human failing cardiomyocytes. *Cardiovasc Res* **62**, 63–73.

MacDonnell SM, García-Rivas G, Scherman JA, Kubo H, Chen X, Valdivia H & Houser SR (2008). Adrenergic regulation of cardiac contractility does not involve phosphorylation of the cardiac ryanodine receptor at serine 2808. *Circ Res* **102**, e65–e72.

Marx SO, Reiken S, Hisamatsu Y, Jayaraman T, Burkhoff D, Rosemblit N & Marks AR (2000). PKA phosphorylation dissociates FKBP12.6 from the calcium release channel (ryanodine receptor): defective regulation in failing hearts. *Cell* **101**, 365–376.

Mika D, Richter W, Westenbroek RE, Catterall WA & Conti M (2014). PDE4B mediates local feedback regulation of β1-adrenergic cAMP signalling in a sarcolemmal compartment of cardiac myocytes. *J Cell Sci* **127**, 1033–1042.

Morimoto S, O-Uchi J, Kawai M, Hoshina T, Kusakari Y, Komukai K, Sasaki H, Hongo K & Kurihara S (2009). Protein kinase A-dependent phosphorylation of ryanodine receptors increases Ca^{2+} leak in mouse heart. *Biochem Biophys Res Commun* **390**, 87–92.

Nikolaev VO, Bünemann M, Schmitteckert E, Lohse MJ & Engelhardt S (2006). Cyclic AMP imaging in adult cardiac myocytes reveals far-reaching β1-adrenergic but locally confined β2-adrenergic receptor–mediated signalling. *Circ Res* **99**, 1084–1091.

Nikolaev VO, Moshkov A, Lyon AR, Miragoli M, Novak P, Paur H, Lohse MJ, Korchev YE, Harding SE & Gorelik J (2010). β2-Adrenergic receptor redistribution in heart failure changes cAMP compartmentation. *Science* **327**, 1653–1657.

Ogrodnik J & Niggli E (2010). Increased Ca^{2+} leak and spatiotemporal coherence of Ca^{2+} release in cardiomyocytes during β-adrenergic stimulation. *J Physiol* **588**, 225–242.

Pereira L, Cheng H, Lao DH, Na L, van Oort RJ, Brown JH, Wehrens XHT, Chen J & Bers DM (2013). Epac2 mediates cardiac β1-adrenergic-dependent sarcoplasmic reticulum Ca^{2+} leak and arrhythmia. *Circulation* **127**, 913–922.

Pereira L, Métrich M, Fernández-Velasco M, Lucas A, Leroy J, Perrier R, Morel E, Fischmeister R, Richard S, Bénitah J-P, Lezoualc'h F & Gómez AM (2007). The cAMP binding protein Epac modulates Ca^{2+} sparks by a Ca^{2+}/calmodulin kinase signalling pathway in rat cardiac myocytes. *J Physiol* **583**, 685–694.

Pereira L, Rehmann H, Lao DH, Erickson JR, Bossuyt J, Chen J & Bers DM (2015). Novel Epac fluorescent ligand reveals distinct Epac1 *vs.* Epac2 distribution and function in cardiomyocytes. *Proc Natl Acad Sci USA* **112**, 3991–3996.

Van Petegem F (2012). Ryanodine receptors: structure and function. *J Biol Chem* **287**, 31624–31632.

Poláková E, Illaste A, Niggli E & Sobie EA (2015). Maximal acceleration of Ca^{2+} release refractoriness by β-adrenergic stimulation requires dual activation of kinases PKA and CaMKII in mouse ventricular myocytes. *J Physiol* **593**, 1495–1507.

Ruiz-Hurtado G, Morel E, Domínguez-Rodríguez A, Llach A, Lezoualc'h F, Benitah J-P & Gomez AM (2013). Epac in cardiac calcium signalling. *J Mol Cell Cardiol* **58**, 162–171.

Shan J, Kushnir A, Betzenhauser MJ, Reiken S, Li J, Lehnart SE, Lindegger N, Mongillo M, Mohler PJ & Marks AR (2010). Phosphorylation of the ryanodine receptor mediates the cardiac fight or flight response in mice. *J Clin Invest* **120**, 4388–4398.

Venetucci L, Denegri M, Napolitano C & Priori SG (2012). Inherited calcium channelopathies in the pathophysiology of arrhythmias. *Nat Rev Cardiol* **9**, 561–575.

Wehrens XHT, Lehnart SE, Reiken SR & Marks AR (2004). Ca^{2+}/calmodulin-dependent protein kinase II phosphorylation regulates the cardiac ryanodine receptor. *Circ Res* **94**, e61–e70.

Wu Y, Luczak ED, Lee E-J, Hidalgo C, Yang J, Gao Z, Li J, H.T. Wehrens X, Granzier H & Anderson ME (2012). CaMKII effects on inotropic but not lusitropic force frequency responses require phospholamban. *J Mol Cell Cardiol* **53**, 429–436.

Xiao B, Sutherland C, Walsh MP & Chen SRW (2004). Protein kinase A phosphorylation at serine-2808 of the cardiac Ca^{2+}-release channel (ryanodine receptor) does not dissociate 12.6-kDa FK506-binding protein (FKBP12.6). *Circ Res* **94**, 487–495.

Xiao B, Tian X, Xie W, Jones PP, Cai S, Wang X, Jiang D, Kong H, Zhang L, Chen K, Walsh MP, Cheng H & Chen SRW (2007). Functional consequence of protein kinase A-dependent phosphorylation of the cardiac ryanodine receptor: sensitization of store overload-induced Ca^{2+} release. *J Biol Chem* **282**, 30256–30264.

Xiao B, Zhong G, Obayashi M, Yang D, Chen K, Walsh MP, Shimoni Y, Cheng H, Ter Keurs H & Chen SRW (2006). Ser-2030, but not Ser-2808, is the major phosphorylation site in cardiac ryanodine receptors responding to protein kinase A activation upon beta-adrenergic stimulation in normal and failing hearts. *Biochem J* **396**, 7–16.

Zaccolo M & Pozzan T (2002). Discrete microdomains with high concentration of cAMP in stimulated rat neonatal cardiac myocytes. *Science* **295**, 1711–1715.

Additional information

Competing interests

None.

Author contributions

K.R.S., E.D. and H.L.R. were involved in designing the experiments and interpreting the data; E.D., D.M.J., S.M.K., G.G. and P.H. collected the data and E.D., D.J.S., G.G. and P.H. analysed the data; K.R.S., E.D., D.J.S., D.M.J., H.L.R., G.G., S.M.K. and P.H. were involved in writing the paper. All authors approved the final version of the manuscript.

Funding

This work was funded by the Interuniversity Attraction Poles P7/10 to K.R.S. and the Research Foundation Flanders (FWO) (project grant to K.R.S.; postdoctoral fellowship to D.M.J. and PhD fellowship to E.D.).

Acknowledgements

We thank Kristel Vermeulen and Dr Ronald Driesen for assistance with animal handling. We also thank Dr Frank Lezoualc'h (INSERM, Toulouse, France) who kindly provided the Epac inhibitor CE3F4.